Ceramics International 52 (2026) 273–285

Contents lists available at ScienceDirect

Ceramics International

journal homepage: www.elsevier.com/locate/ceramint

Thermoluminescence study of $YBa_3(BO_3)_3$: Trap characterization and kinetic parameters via multi-method analysis

E. Aymila Çin [a], K. Bulcar [b], Jabir Hakami [c], U.H. Kaynar [d], M. Sharahili [c], O. Madkhali [c], D. Somaily [c], Rachid Karmouch [c], D.A. Jabali [c], M.B. Coban [e], G.M. Güngör Price [f], M. Topaksu [f], N. Can [c,*]

[a] Bakırcay University, Graduate School of Natural and Applied Sciences, Menemen, Izmir, Türkiye
[b] Igdir University, Vocational School of Health Services, Karaagac Campus, 76000, Igdir, Türkiye
[c] Jazan University, College of Science, Department of Physical Sciences, Physics Division, P.O. Box 114, 45142, Jazan, Saudi Arabia
[d] Bakırcay University, Faculty of Engineering and Architecture, Department of Fundamental Sciences, Menemen, Izmir, Türkiye
[e] Balikesir University, Faculty of Arts and Sciences, Department of Physics, Balikesir, Türkiye
[f] Physics Department, Cukurova University, Arts-Sciences Faculty, 01330, Adana, Türkiye

ARTICLE INFO

Keywords:
$YBa_3(BO_3)_3$
Thermoluminescence
Trap parameters
Glow curve deconvolution

ABSTRACT

The thermoluminescence (TL) properties of $YBa_3(BO_3)_3$ phosphor were systematically investigated to evaluate its trap characteristics and potential for radiation dosimetry applications. TL glow curves recorded at various heating rates (0.5–10 °C/s) exhibited two prominent peaks with unusually stable intensities, contrary to conventional TL behavior. T_M–T_{stop} analysis revealed a complex trap structure composed of both continuous and discrete energy levels, with activation energies ranging from 1.21 to 1.91 eV, identified via the initial rise method. The impact of preheating on trap population was examined, highlighting the thermal instability of shallow traps and the robustness of deeper ones. Kinetic parameters such as activation energy, frequency factor, and kinetic order were extracted using the Variable Heating Rate (VHR) method and Computerized Glow Curve Deconvolution (CGCD). For preheated glow curves, deconvolution was carried out using a first-order kinetic model ($b = 1$), as supported by recent simulation studies. The resulting fits showed well-isolated deep glow peaks with activation energies between ~1.12 and ~1.95 eV, in agreement with other analytical methods. The results thus confirm first-order kinetic behavior across all preheated glow curves, consistent with the stable peak positions and reliable fitting outcomes. These findings demonstrate that undoped $YBa_3(BO_3)_3$ hosts thermally stable deep traps and exhibits minimal recombination loss under rapid heating, rendering it a promising candidate for high-performance TL dosimetry.

1. Introduction

Rare-earth doped luminescent materials have attracted extensive research interest in recent decades owing to their superior luminescence efficiency, excellent chemical and thermal stability, and wide applicability in solid-state lighting, optoelectronic devices, and radiation dosimetry [1–7]. Among the techniques employed to investigate such materials, thermoluminescence (TL) stands out as a highly sensitive and non-destructive method for exploring defect-related trapping and recombination processes induced by radiation exposure [8–10]. TL measurements provide insight into the energetic structure of traps and recombination centers, often revealing crucial information about the kinetic parameters and structural integrity of phosphor materials [10].

Host matrices incorporating borate groups, particularly aluminoborates, have shown notable potential in TL applications due to their large bandgap, low phonon energy, and high thermal resistance, which make them ideal for rare-earth doping and efficient radiative transitions [11–13]. For example, $YAl_3B_4O_{12}$ (YAB) doped with Eu^{3+}, Sm^{3+} or Tb^{3+} ions exhibits well-defined TL glow peaks, high reproducibility, and favorable trapping characteristics under ionizing radiation. These systems also demonstrate complex kinetic behaviors, including peak shifting and trap saturation phenomena, dependent on dopant concentration and synthesis route.

Despite considerable progress in the development of aluminoborate-

* Corresponding author.
E-mail address: ncan@jazanu.edu.sa (N. Can).

https://doi.org/10.1016/j.ceramint.2025.11.316
Received 10 October 2025; Received in revised form 10 November 2025; Accepted 22 November 2025
Available online 25 November 2025

based phosphors, borate compounds with alternative cationic frameworks—such as YBB—have received little attention in thermoluminescence research. While the BO_3 trigonal planar network of $YBa_3(BO_3)_3$ (YBB) broadly resembles that of $YAl_3(BO_3)_3$ (YAB), the substitution or incorporation of larger divalent Ba^{2+} ions into the lattice introduces a pronounced ionic radius and valence mismatch relative to trivalent Y^{3+}. This mismatch can induce local lattice distortion, internal strain, and charge-compensation mechanisms that are known to influence defect chemistry in ceramic hosts. Although there exists no universally predictive model for thermoluminescence (TL) behavior solely based on crystal structure, several studies have reported that such structural perturbations can modify trap formation and affect the energy depth and thermal stability of charge trapping centers.

For instance, in ZnO:RE phosphors, rare-earth doping has been shown to introduce lattice distortion due to ionic size mismatch, which in turn impacts the distribution of trapping defects and TL response (Manju et al., 2021). Similar observations were made by Vu et al. (2023), who found that substitution of Mg^{2+} by larger Dy^{3+} ions in $MgAl_2O_4$ spinels led to measurable changes in luminescence and TL behavior, attributed to the altered crystal field environment. From a computational perspective, Zhydachevskyy et al. (2021) demonstrated that local lattice dilation or compression surrounding intrinsic point defects in perovskites can modulate trap depths and band gap width. Likewise, Bork et al. (2017) revealed that in $BaZrO_3$ systems, the mismatch between dopant and host ionic radii significantly alters the energy landscape experienced by mobile defect species.

Given this context, it is reasonable to hypothesize that the altered structural environment in YBB, induced by Ba^{2+} incorporation, may promote the stabilization of deeper or more thermally stable trapping centers, thereby influencing its TL performance. This hypothesis is further examined through experimental kinetic analysis and glow curve deconvolution presented in the current study.

This altered structural environment could potentially foster deeper, more thermally stable trapping centers favorable for TL emission. Furthermore, the presence of heavier alkaline earth elements such as barium has been shown in various host lattices to modulate trap creation, trap depth distribution, and recombination efficiency through mechanisms such as local lattice distortion, ionic radius mismatch, and induced strain fields, all of which play a critical role in the thermal stability and kinetic behavior of TL-active centers [14,15]. Given these structural and compositional features, YBB presents itself as a promising but hitherto unexplored candidate for advanced TL dosimetric applications, especially in the context of rare-earth-free or intrinsic trap-dominated systems. In this work, we present the first comprehensive investigation of the thermoluminescent properties of YBB phosphors synthesized via a solution combustion route.

The study focuses on the characterization of trapping states induced by β-irradiation using a suite of TL techniques, including the initial rise (IR) method, variable heating rate (VHR) analysis, and computerized glow curve deconvolution (CGCD). These approaches allow for the extraction of kinetic parameters such as activation energy, frequency factor, and kinetic order, thereby offering a detailed understanding of the charge carrier dynamics within the host matrix. Furthermore, the T_M–T_{stop} protocol was employed to resolve overlapping glow peaks and to identify suitable kinetic models corresponding to thermally activated recombination processes. The findings not only contribute to the fundamental understanding of trap structure in YBB but also underscore its potential relevance in the development of borate-based TL dosimeters.

2. Experiments

Analytical-grade starting materials were used for the synthesis of YBB phosphors. Yttrium (III) oxide (Y_2O_3, 99.8 %, Sigma-Aldrich), barium nitrate ($Ba(NO_3)_2$, 99.99 %, Sigma-Aldrich), and boric acid (H_3BO_3) served as the principal oxidizing agents. In the combustion reaction, urea ($CO(NH_2)_2$) and glycine ($C_2H_5NO_2$) were introduced as fuels to facilitate gel formation and promote homogeneity. To prepare the precursor solution, Y_2O_3 was first dissolved in diluted nitric acid to obtain a clear $Y(NO_3)_3$ solution. The stoichiometric ratios of $Y(NO_3)_3$, $Ba(NO_3)_2$, and H_3BO_3 were carefully calculated according to the YBB molar formula, and the components were mixed thoroughly in an agate mortar with minimal deionized water to obtain a uniform slurry. The resulting gel was dried at 120 °C overnight to eliminate residual moisture and ensure complete nitrate formation. Following gelation, the dried mass was subjected to a solid-state heat treatment process. A pre-calcination step at 600 °C for 4 h in air was conducted to remove volatile organics and decompose residual precursors. The intermediate product was then ground and sintered at 950 °C for 6 h to induce crystallization and phase stabilization. After furnace cooling to room temperature, the final powders were stored in airtight containers to prevent moisture uptake. This combustion-assisted solid-state synthesis approach yielded high-purity YBB powders with good crystallinity and phase purity. The method was specifically optimized to eliminate the use of rare-earth dopants, allowing the investigation of intrinsic TL behavior associated with native defect centers in the host lattice.

The phase composition and crystal structure of the synthesized YBB powders were examined via powder *X*-ray diffraction (XRD) using a Bruker D8 Advance diffractometer equipped with Cu Kα radiation (λ = 1.5406 Å). The diffraction data were collected over the 2θ range of 10°–70° at a step size of 0.02°, and a scan rate optimized to ensure high signal-to-noise resolution.

Thermoluminescence (TL) measurements were carried out using a Lexsyg Smart TL/OSL reader equipped with a calibrated $^{90}Sr/^{90}Y$ beta radiation source operating at a dose rate of approximately 0.097 Gy/s. For each measurement, about 10.4 mg of the YBB powder was compressed into 6 mm diameter pellets using a manual hydraulic press to ensure uniform sample geometry and reproducible thermal contact. Glow curves were recorded by heating the irradiated samples from ambient temperature up to 450 °C under a linear heating regime. The standard heating rate was set to 2 °C/s; however, to systematically explore thermal transport effects on the TL emission profile, additional measurements were conducted at variable heating rates ranging from 0.5 °C/s to 10 °C/s. All measurements were performed under a nitrogen purge to suppress oxidative effects and minimize spurious signals. Background correction was rigorously applied to all glow curves by subtracting both dark counts and natural background signals, which were acquired from non-irradiated control samples under identical conditions. The irradiated phosphor pellets were stored in light-tight containers and handled under red-light conditions to avoid any premature charge release from shallow traps. Although the samples were synthesized as fine powders, a brief manual mixing using an agate mortar was performed before pellet pressing to promote homogeneity and reduce the likelihood of triboluminescence artifacts caused by friction between irregular particles. This measurement protocol ensured accurate characterization of TL features intrinsic to the YBB lattice, providing reliable data for subsequent kinetic analysis and trap parameter extraction.

3. Results and discussions

3.1. Structural characterization by X-ray diffraction

The obtained XRD pattern (Fig. 1) displays sharp and well-defined diffraction peaks, all of which can be indexed to the hexagonal phase of YBB, consistent with the standard JCPDS reference pattern (card no. 98-009-9180) [16]. No additional peaks attributable to secondary phases or residual precursors were detected, indicating successful synthesis of a phase-pure material. All observed reflections conform to the space group R32, characteristic of borate frameworks with layered BO_3 units interconnected through Y and Ba cation coordination. The absence of any peak splitting or broadening confirms the structural integrity and

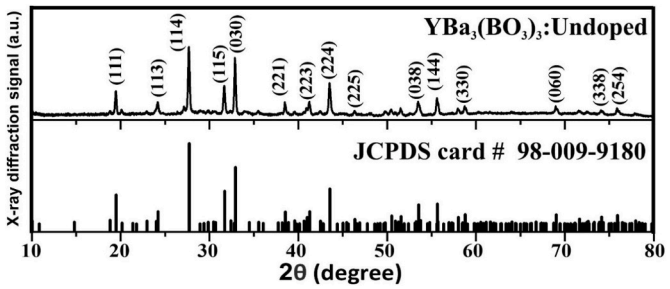

Fig. 1. Powder X-ray diffraction (XRD) pattern of YBB phosphor synthesized via combustion-assisted solid-state reaction.

high crystallinity of the lattice. These results affirm that the adopted synthesis protocol effectively yields single-phase YBB with no apparent crystallographic defects or dopant-induced distortions, laying a stable foundation for subsequent TL investigations centered on intrinsic defect-related phenomena.

3.2. Spectral filter analysis of TL emission

To assess the spectral response and temperature-dependent behaviour of the TL response, YBB phosphors were β-irradiated to 20 Gy, and their TL glow curves were recorded using four detection windows integrated into the Lexsyg Smart system: BSL-TL (365 nm), IRSL-TL (410 nm), IRSL-TL (565 nm), and IRSL-TL wideband blue [17].

As illustrated in Fig. 2, all detection windows revealed the main TL features, with two clear glow maxima centered around 90 °C and 290 °C, corresponding to shallow and deep traps, respectively. Among the tested filters, the IRSL-TL wideband blue configuration yielded the highest sensitivity and signal-to-noise ratio, resulting in more clearly resolved and thermally stable glow features. To highlight weak shoulders and low-intensity components, the TL glow curves were additionally plotted on a logarithmic intensity scale, following the approach recommended by Can et al. [18]. This representation allows subtle peak shifts and secondary maxima to be resolved more clearly than in standard linear plots. The 410 nm and 565 nm bandpass filters, being narrower, showed reduced intensity due to their limited spectral transmittance, while the

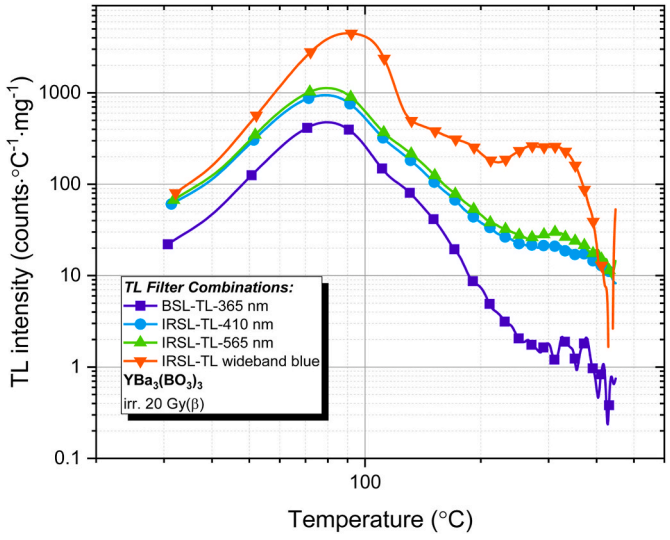

Fig. 2. TL glow curves of YBB phosphor recorded under different optical filter combinations after β-irradiation to 20 Gy. The IRSL-TL wideband blue filter provided the strongest signal intensity and enabled better resolution of shallow and deep traps, as visualized on a logarithmic intensity scale. (For interpretation of the references to colour in this figure legend, the reader is referred to the Web version of this article.)

365 nm filter captured only a small fraction of the broad visible emission.

Since the purpose of this study was to evaluate the TL response as a function of temperature, rather than to perform a detailed wavelength-resolved analysis, the wideband blue filter was selected for quantitative comparison and kinetic evaluation. The enhanced response in this channel indicates that the emission from YBB is broadly distributed within the visible range, particularly between 340 nm and 490 nm, consistent with intrinsic defect-related recombination in borate hosts synthesized by combustion.

These results demonstrate that the wideband blue filter effectively captures the dominant TL emission, ensuring high-signal-to-noise ratio measurements suitable for reliable I–T analysis and comparison among samples, while the other filters provide confirmatory spectral context for emission coverage.

3.3. Preheating optimization for TL signal stability

In thermoluminescence dosimetry, the implementation of a preheating step prior to glow curve acquisition is a well-established method to eliminate unstable shallow traps that may contribute to spurious low-temperature signals [19]. To determine an appropriate, preheat temperature for YBB phosphors, a systematic preheat protocol was applied following β-irradiation at 20 Gy.

Each cycle involved initial heating of the sample to a specific preheat temperature ranging from 50 °C to 250 °C (in 5 °C increments) at a linear rate of 2 °C/s, followed by rapid cooling to room temperature. Subsequently, the sample was reheated from RT to 450 °C to record the residual TL glow curve. The integrated TL intensity was plotted as a function of the preheat temperature (Fig. 3a). As observed, a sharp decrease in total TL signal occurs in the 50–160 °C region, indicating the progressive removal of low-temperature, thermally unstable trap populations.

The TL signal reaches a plateau beyond 155 °C, indicating the thermal depletion of unstable shallow traps and stabilization of the remaining deeper trap population, in agreement with classical preheating principles described by McKeever [9]. Therefore, 155 °C was selected as the optimum preheat temperature, balancing signal stability and retention of deeper trap information. This preheat setting ensures that subsequent TL analyses reflect only thermally stable trap levels, enabling more reliable kinetic characterization.

To validate the influence of heating time, a fixed preheat temperature of 155 °C was applied with varying preheat durations from 1 to 9 *s*. As shown in Fig. 3b, the integrated TL intensity remained stable between 1 and 5 *s* and then exhibited a noticeable decline beyond 6 *s*, likely due to partial annealing of deeper traps. Thus, a preheat duration of 5 *s* was adopted to preserve the signal from kinetically relevant trap centers while minimizing shallow trap interference. Insets in Fig. 3a and b shows the corresponding TL glow curves with and without preheating, further confirming the selective depletion of shallow traps.

3.4. Dose response behavior

The dose dependence of thermoluminescence (TL) response offers crucial insight into the trap filling dynamics and practical dosimetric range of a phosphor. Fig. 4a presents the TL glow curves of undoped YBB recorded after β-irradiation doses ranging from 1 to 500 Gy. The glow curve shape and peak position remain nearly unchanged with increasing dose—behavior commonly associated with first-order kinetic processes—while the intensity increases proportionally. Accordingly, the glow curve deconvolution was performed using a first-order kinetic model, which reduced parameter ambiguity in overlapping regions and yielded consistent trap parameters across different dose levels, supporting the validity of this simplified kinetic approach.

To assess the functional dependence of TL signal on dose, the integrated TL area was plotted in log–log coordinates (Fig. 4b). Two distinct

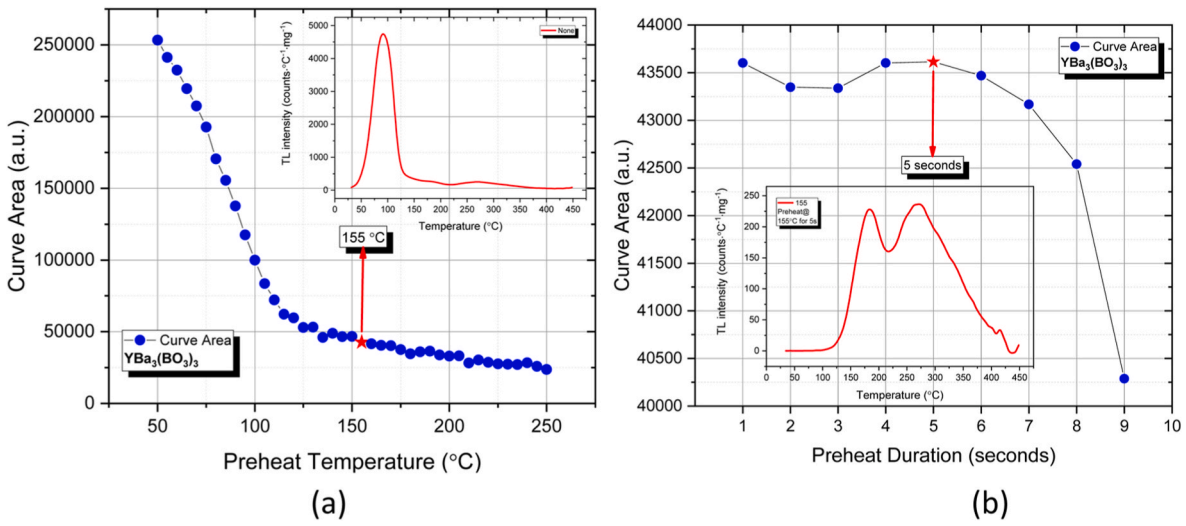

Fig. 3. (a) Integrated TL intensity vs. preheat temperature for YBB. A plateau beyond 155 °C indicates depletion of shallow traps and stabilization of deeper ones. (b) TL intensity vs. preheat duration at 155 °C. Signal remains stable up to 5 *s*, then decreases due to possible annealing of deeper traps.

regions were analyzed using a power-law fitting model of the form $I = a{\cdot}D^b$. For the low-to-mid dose range (1–150 Gy), the response exhibits near-ideal linearity with an exponent $b = 1.007$ and a high correlation coefficient $R^2 = 0.99927$, indicating a proportional increase in trap occupancy without significant competition or saturation effects.

Beyond 150 Gy, however, the dose response deviates from linearity, transitioning into a sublinear regime with $b = 0.85$ and $R^2 = 0.99825$. This behaviour suggests the onset of trap saturation, consistent with models proposed by McKeever [9], wherein deeper traps begin to dominate the recombination kinetics and reduce the marginal TL output per unit dose. Bos [20] similarly noted that such deviations may also reflect experimental nonlinearities including partial retrapping, carrier depletion, or readout-induced bleaching at high doses.

The ability of YBB to maintain a near-linear TL response up to ~150 Gy positions it favourably among potential dosimetric materials, especially for mid-dose range applications. The observed sublinearity at higher doses is gradual rather than abrupt, implying a well-behaved trap distribution without over-response or anomalous recombination effects.

3.5. Stability and reusability of YBB phosphors

The stability and reusability of YBB phosphors were systematically evaluated by subjecting the samples to ten consecutive irradiation–readout cycles using a constant β-dose of 100 Gy. Between each cycle, high-temperature annealing was employed to ensure complete signal erasure. Fig. 5a–c presents the normalized thermoluminescence (TL) peak intensities corresponding to Peak I (~180 °C), Peak II (~268 °C), and the total integrated glow-curve area as a function of readout order.

The data reveal excellent reproducibility in TL response across successive cycles. Specifically, Peak I displayed a maximum deviation of ±0.87 %, while Peak II varied by only ±0.62 % relative to their initial values. The integrated TL intensity remained within ±0.58 % of its mean value, well below the ±5 % acceptance threshold typically considered indicative of dosimetric reliability [21]. In addition to amplitude stability, the glow-peak positions showed minimal drift ($\Delta T_m < 2$ °C), confirming that the trapping and recombination mechanisms remained thermally robust and unaffected by repeated readouts. These findings suggest that the shallow and deeper trapping states in YBB are structurally stable and resilient to thermal cycling. Taken together, these results demonstrate that YBB phosphors possess outstanding cycle-to-cycle stability, low signal loss, and minimal trap redistribution—key characteristics for practical TL dosimetry applications, particularly in scenarios requiring material reuse without recalibration.

3.6. Influence of unusual heating rate on the thermoluminescence response

To evaluate the kinetic behavior of charge carrier release in the YBB phosphor, TL glow curves were acquired at multiple linear heating rates ranging from 0.5 °C/s to 10 °C/s following β-irradiation at 100 Gy. All samples underwent a standardized preheat treatment at 155 °C for 5 s to eliminate unstable shallow traps prior to readout.

As presented in Fig. 6a, the glow curves consistently exhibit two main peaks: Peak I centered near 163 °C and Peak II near 240 °C (for 0.2 °C/s heating rate). As expected, increasing the heating rate causes a systematic shift in the glow maxima (T_m) to higher temperatures, attributable to the thermally driven acceleration of carrier release and minor temperature lag within the sample matrix.

To correct for this temperature lag effect and enable accurate comparison of T_m values across different heating rates, a logarithmic interpolation method was applied using the following empirical relation:

$$T_{m_j} = T_{m_i} - \frac{T_{m_2} - T_{m_1}}{ln\left(\frac{\beta_2}{\beta_1}\right)} ln\left(\frac{\beta_i}{\beta_j}\right)$$

where T_m is the corrected peak temperature at heating rate β_j, and T_{m1}, T_{m2} are peak temperatures observed at reference rates β_1, β_2. This correction minimizes thermal lag artifacts and reveals the intrinsic thermally stimulated behavior of the traps.

However, what distinguishes the current material system from conventional TL behaviour is the striking thermal stability of the peak intensities.

In most TL phosphors, increasing the heating rate leads to a noticeable decline in TL intensity due to reduced dwell time at lower temperatures and inefficient recombination. Contrarily, Fig. 6b illustrates that I_{m1} (Peak I intensity) shows a slight increasing trend across the tested range, while I_{m2} (Peak II intensity) remains nearly constant, with fluctuations within ±5 %. This behaviour is particularly pronounced at low heating rates: for example, Peak I appears at 162 °C ($I_{m1} = 1534$ a.u.) at 0.5 °C/s and shifts to 173 °C ($I_{m1} = 1534$ a.u.) at 0.5 °C/s, with negligible change in intensity. Similar stability is observed at higher rates up to 10 °C/s.

Such unusual heating rate dependence aligns with earlier reports on borate-based and other oxide phosphors exhibiting thermally robust trapping structures [12,22]. The results suggest that YBB possesses deep,

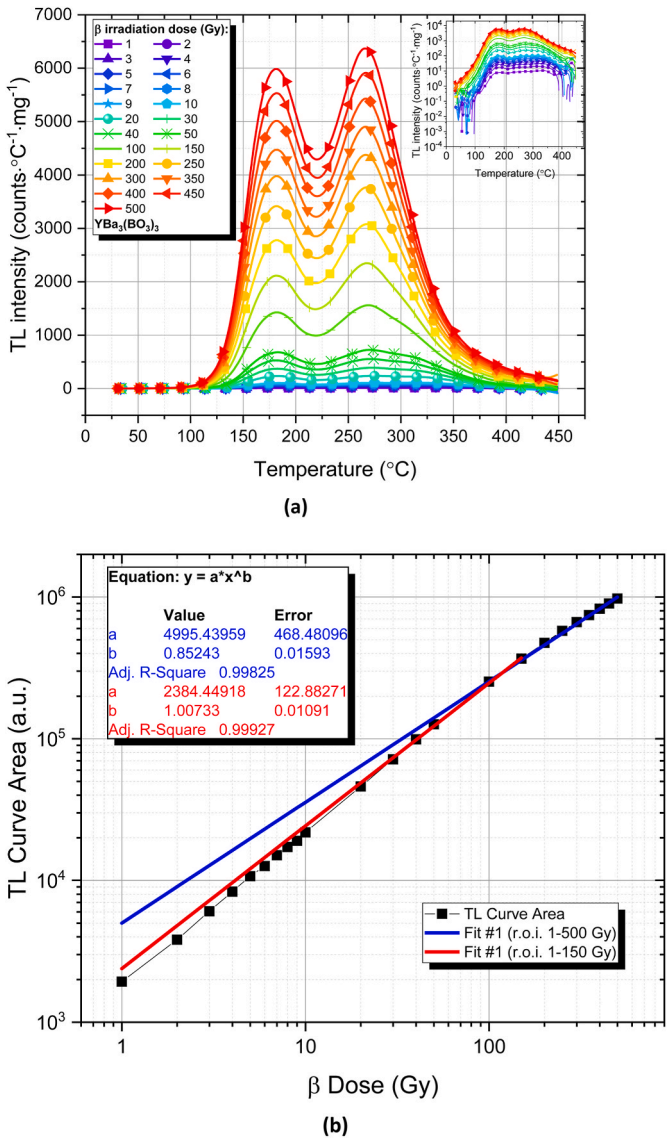

Fig. 4. (a) TL glow curves of $YBa_3(BO_3)_3$ phosphor irradiated with β doses from 1 to 500 Gy. The intensity increases with dose, while glow peak positions remain stable.(b) Dose–response curve (log–log) showing linearity up to 150 Gy and supralinearity beyond, fitted using power-law functions.

well-isolated traps with high thermal retention and low retrapping probability, leading to minimal recombination losses under rapid heating. Additionally, the efficient heat transfer properties of the host matrix may suppress temperature gradient effects, further stabilizing the TL response.

These findings support the interpretation that the TL behavior in YBB deviates from first-order kinetics typically observed in simpler hosts and instead reveals a more complex trap-release mechanism resilient to changes in thermal ramping. This makes the material a promising candidate for applications requiring heating-rate-independent dosimetric reliability.

As presented in Fig. 6c, the glow curves consistently exhibit two main peaks: Peak I centered near 163 °C and Peak II near 240 °C (for 0.2 °C/s heating rate). As expected, increasing the heating rate causes a systematic shift in the glow maxima (T_m) to higher temperatures, which is primarily attributed to the thermally driven acceleration of carrier release. However, this shift is also significantly influenced by the temperature lag effect, whereby the sample's internal temperature lags behind the programmed value due to finite thermal conductivity and heat transfer delays. This phenomenon, quantified using the expression provided by Kitis and Tuyn [23], is illustrated in Fig. 6c, showing that T_m values corrected for thermal lag are consistently lower than the observed values, particularly at high heating rates. For instance, Peak I experiences a temperature lag of approximately 6.8 °C at 5 °C/s and 22.3 °C at 10 °C/s, both of which are non-negligible and must be accounted for in accurate kinetic modelling.

4. Kinetic characterization of thermoluminescence peaks

TL materials exhibit complex carrier dynamics, with charge release mechanisms often governed by a distribution of trap depths and activation energies. To elucidate these kinetic parameters, several analytical models have been developed based on the thermal behavior of glow peaks. Among these, the variable heating rate (VHR) technique offers a practical and effective approach to extract activation energies and frequency factors by analyzing glow peak shifts under different thermal ramping conditions.

The VHR approach rests on the premise that each TL glow peak arises from an ensemble of traps characterized by distinct kinetic parameters. Accordingly, by conducting TL measurements at multiple heating rates and tracking the corresponding peak temperatures, one can determine the activation energy E from the shift in peak maxima, while also estimating the frequency factor s. The methodology becomes particularly powerful when combined with temperature lag corrections and dual-rate comparisons, enhancing the reliability of the extracted kinetic parameters.

4.1. Various heating rate (VHR) method

The kinetic analysis in this study employs the conventional formulation of the VHR method introduced by Hoogenstraaten [24], which is based on plotting $ln(T_m^2/\beta)$ against $1/k_B T_m$, where β is the linear heating rate and T_m the peak temperature at each rate. This linearized form allows estimation of the activation energy E from the slope and the frequency factor s from the intercept of the plot. The mathematical relations used in this method have been discussed in detail in our recent studies [25,26]. The expression is given by:

$$E = k \cdot \frac{T_{m1} T_{m2}}{T_{m1} - T_{m2}} \cdot ln\left(\frac{\beta_1}{\beta_2} \cdot \left(\frac{T_{m2}}{T_{m1}}\right)^2\right)$$

Although this equation is often associated with the simplified two-point Booth–Bohun–Porfianovitch (BBP) method [27,28], it is equally valid within the broader VHR framework introduced by Hoogenstraaten, especially when comparing two distinct heating rates. This conceptual overlap highlights the mathematical consistency of both approaches in evaluating activation energies from temperature-dependent TL data.

This two-point method enables the calculation of E using two distinct heating rates (β_1, β_2) and their corresponding peak temperatures (T_{m1}, T_{m2}). While the approach assumes first-order kinetics, it is broadly applicable across many TL systems, particularly when combined with thermal lag corrections that account for deviations due to sample heat transfer inefficiencies.

However, due to the intrinsic thermal lag between the programmed and actual sample temperature during TL readout, especially at high heating rates, the measured T_m values may deviate significantly from the true values. To address this, the temperature lag correction (TLA) approach proposed by Kitis and Tuyn [23] was applied prior to VHR analysis. This correction ensures more accurate kinetic parameter extraction by compensating for the thermal delay inherent to the heating system.

In this study, the VHR method was applied to Peak I and Peak II of YBB using both raw and TLA-corrected peak temperatures. A detailed evaluation of these results, together with a direct comparison to the two-

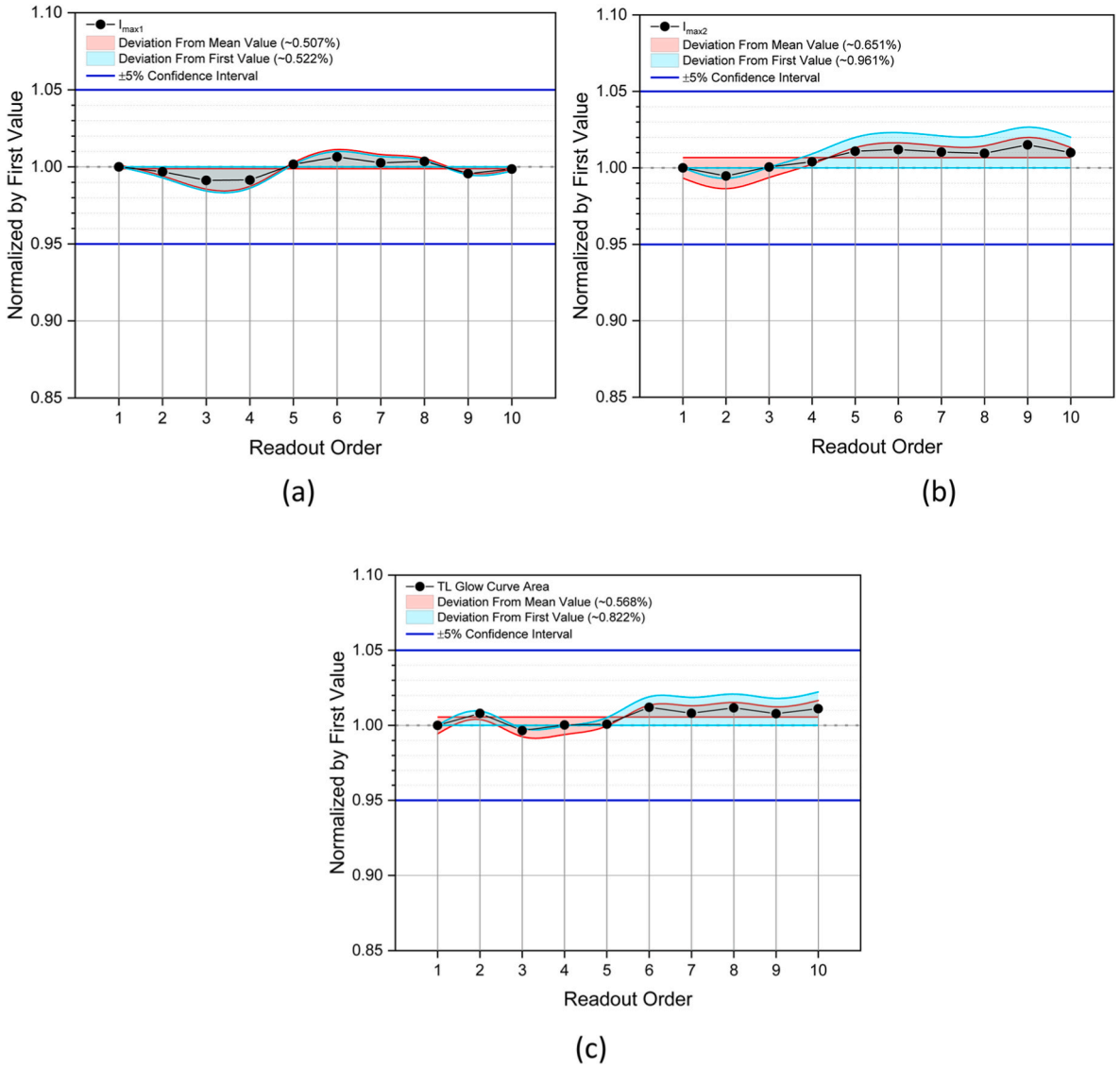

Fig. 5. Stability and reusability assessment of $YBa_3(BO_3)_3$ phosphors over ten consecutive β-irradiation–readout cycles at 100 Gy. (a) Normalized peak intensity of TL Peak I (~180 °C); (b) Normalized intensity of TL Peak II (~268 °C); and (c) Total integrated TL glow-curve area, normalized to the first readout.

point heating rate method—commonly referred to as the Booth–Bohun–Porfianovitch method [27,28]—is provided in Table 1. These methods were used to calculate the activation energy (E) and frequency factor (s) across different heating rates ranging from 0.5 to 10 °C/s.

As shown in Table 1 and Fig. 7a–b, incorporating thermal lag corrections leads to a significant increase in the calculated activation energies. For Peak I, the average E rises from 1.15 eV (uncorrected) to 1.37 eV (corrected), while for Peak II, it increases from 1.21 eV to 1.40 eV. This trend is consistent across all heating rates analyzed. Notably, the frequency factors also change by several orders of magnitude, reflecting improved accuracy after lag compensation.

These findings highlight the importance of incorporating thermal lag considerations when performing kinetic analysis on glow curves measured under variable heating rates. Failure to correct for such effects may lead to underestimation of activation energies and misinterpretation of trap characteristics. The comparative results using the BBP method also support the robustness of the VHR approach under both uncorrected and corrected conditions.

4.2. Comparison of preheated and non-preheated T_m–T_{stop} analyses

The T_M–T_{stop} method, originally introduced by McKeever [9], was applied to investigate the trap characteristics of YBB. This method involves heating the sample to a selected stop temperature (T_{stop}), then cooling and reheating to record the TL glow curve. In this study, the procedure was implemented without any preheating step, allowing the direct observation of thermally stimulated glow peaks across a wide range of intermediate temperatures.

The sample was irradiated with 20 Gy and heated from room temperature to T_{stop} values ranging from 50 °C to 365 °C in 5 °C increments. Following each T_{stop}, the sample was cooled to room temperature, and a subsequent TL glow curve was recorded. The evolution of the TL glow curves is shown in Fig. 8a, while the variation of the glow peak temperature (T_M) as a function of T_{stop} is presented in Fig. 7b.

The T_M–T_{stop} plot shown in Fig. 8 b reveals three distinct regions. Between 50 and 120 °C, a nearly linear increase in T_M with T_{stop} suggests a continuous distribution of traps. A plateau-like region follows between ~120 and 210 °C, indicating a more discrete set of thermally stable traps with fixed activation energies. the slope increases again, suggesting the presence of deeper or partially overlapping trap levels—consistent with

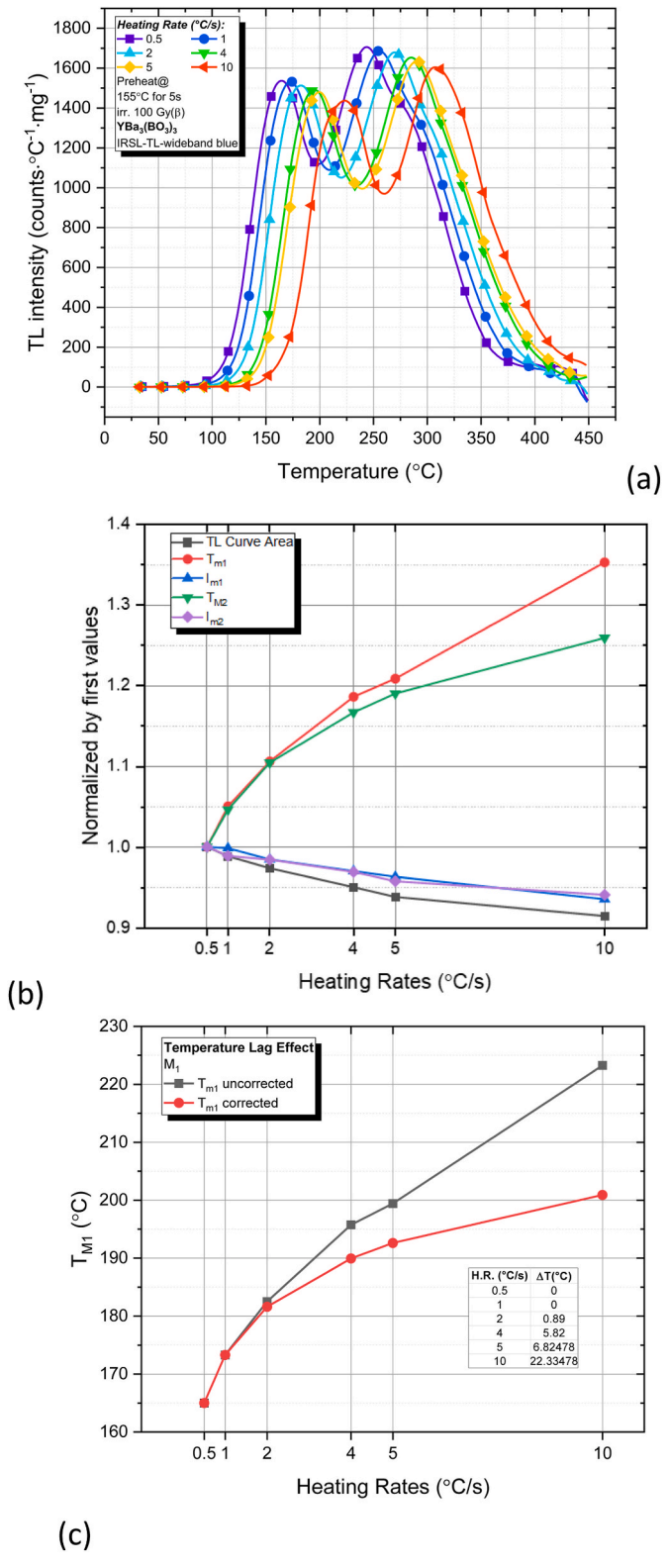

Fig. 6. (a) TL glow curves of YBB at different heating rates. (b) Peak intensities (I_{m1} and I_{m2}) versus heating rate. (c) Corrected and uncorrected T_m values showing temperature lag effect.

prior findings in borate-based phosphors such as LaB_3O_6:Tb^{3+} and $Li_2B_4O_7$:Cu,Ag [29,30]. These results support the multilevel trap nature of the material, further corroborated by first-order CGCD analysis across multiple doses.

To complement this analysis, trap depths (E) were calculated using the initial rise (IR) method, based on the assumption that the early part of the glow curve follows an exponential trend [31]. Fig. 8c displays the derived activation energies as a function of T_{stop}, revealing the energy distribution of traps across the temperature range. Several distinct energy levels were identified: shallow traps around 0.78–1.07 eV dominate the low T_{stop} range (<120 °C), while deeper traps emerge progressively between 1.3 and 1.78 eV at intermediate T_{stop} values (150–290 °C). Notably, a high-energy trap cluster around 2.05–2.08 eV appears beyond 300 °C, indicating the presence of deep, thermally stable traps.

These findings suggest that YBB contains a complex mixture of shallow and deep traps, some with broad energy distributions and others with discrete energy levels. This multilevel structure supports the material's potential for radiation storage and dosimetry applications, consistent with similar behaviors observed in rare-earth doped borate hosts [29].

To further resolve the underlying trap structure of YBB, the T_m–T_{stop} experiment was repeated following a preheating step, in which the sample was initially annealed to 155 °C for 5 *s* prior to each T_{stop} cycle. This pre-irradiation heating was designed to empty low-energy shallow traps and isolate the behavior of more thermally stable traps by suppressing early TL emissions.

The resulting trap depth analysis, illustrated in Fig. 8d, reveals a markedly different profile compared to the non-preheated case. In the lower T_{stop} region (<150 °C), the initial rise method yields significantly reduced activation energy values and fewer defined trap levels, confirming the effective removal of shallow traps during preheating. As T_{stop} increases, a more pronounced emergence of deeper traps becomes evident. Between ~200 and 310 °C, dominant energy levels at 1.32, 1.37, and 1.51 eV become more sharply resolved. Above 310 °C, the appearance of high-energy traps around 2.06–2.08 eV persists, consistent with the unheated results, indicating their inherent thermal stability and resistance to prior annealing steps.

Notably, the suppression of overlapping lower-energy traps results in a more clearly segmented trap structure, where each energy level appears more distinct and less influenced by adjacent distributions. The high degree of consistency in deep-level trap energies across both preheated and non-preheated analyses supports the validity and reproducibility of these results.

Overall, a comparative evaluation of the two approaches underscores their complementary nature. The non-preheated method allows the mapping of the full trap distribution, including shallow and thermally unstable states, while the preheated method selectively enhances the visibility of deeper, persistent traps by minimizing thermal interference. Together, these methods provide a more comprehensive understanding of the trapping system in YBB, revealing its suitability for high-temperature dosimetric applications where thermal stability is critical.

4.3. Glow curve deconvolution analysis

The glow curve of thermoluminescence (TL) typically consists of several overlapping peaks, each associated with different trapping and recombination mechanisms, including trapped charge carriers, recombination centers, and retrapping processes. To resolve these overlapping features and extract kinetic parameters such as trap depth (E), frequency factor (s), and kinetic order (b), computerized glow curve deconvolution (CGCD) is employed. This approach allows the TL glow curve to be modelled as a linear combination of individual peaks using mathematical functions that reflect the physical nature of the trapping processes.

Various studies have proposed combinations of exponential, Gaussian, and general-order kinetics functions to fit TL glow curves effectively [29]. This modelling allows not only for the determination of kinetic parameters but also accounts for complex processes such as retrapping and recombination effects. While general-order kinetics is often employed for materials with overlapping TL peaks, in this study, a first-order kinetic model was specifically adopted to minimize parameter ambiguity and align with the observed invariance of TL glow peak

Table 1
Activation energies (E) and frequency factors (s) calculated for two TL maxima using the Booth-Bohun-Parfianovitch (BBP) and Hoogenstraaten's methods at different heating rates (β), comparing uncorrected and temperature-lag-corrected T_M values.

β (°C/s)	*Maximum 1*		*Maximum 2*		
	UnCorrected	*Corrected*	*UnCorrected*	*Corrected*	
1	1.33	1.33	1.35	1.35	Booth-Bohun-Parfianovitch (BBP)
2	1.29	1.36	1.22	1.38	
4	1.12	1.38	1.18	1.41	
5	1.11	1.39	1.15	1.42	
10	0.88	1.41	1.13	1.45	
Average E	1.15 ± 0.18	1.37 ± 0.03	1.21 ± 0.09	1.40 ± 0.04	
***E* (eV)**	0.89 ± 0.09	1.41 ± 0.02	1.12 ± 0.03	1.45 ± 0.02	Hoogenstraaten's Method
(0.5–10 °C/s)					
***s* (s^{-1})**	6.06×10^{8}	7.28×10^{14}	2.10×10^{9}	4.12×10^{12}	

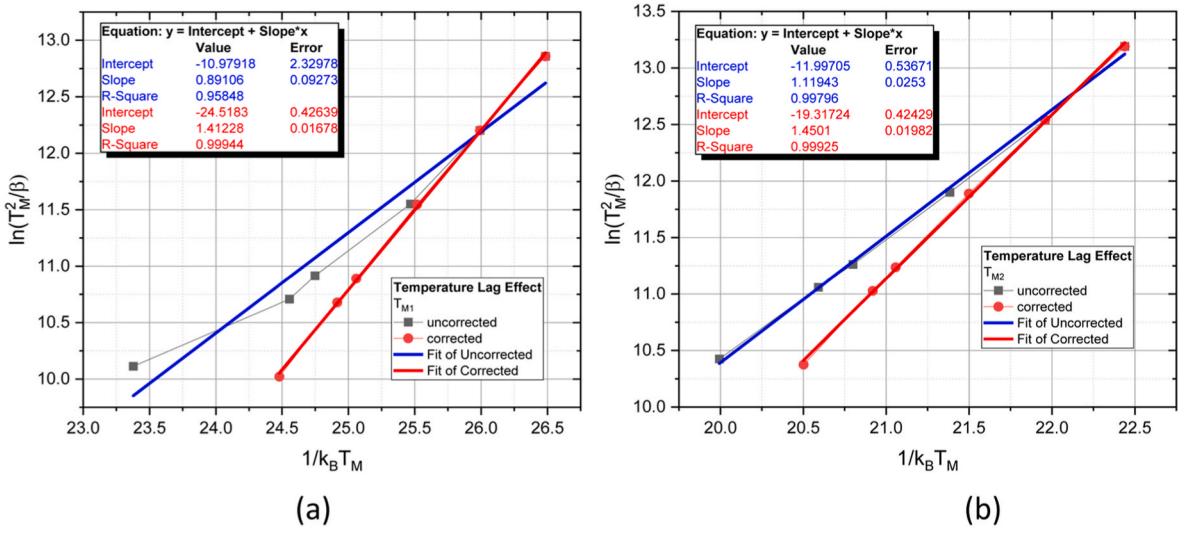

Fig. 7. Linearized plots of ln (T_m^2/β) versus $1/k_B T_m$ for (a) Peak I and (b) Peak II, using both uncorrected and thermal-lag-corrected T_m values. The slopes and intercepts obtained from linear fits were used to extract activation energy (E) and frequency factor (s) based on the Hoogenstraaten VHR method.

positions with dose. This approach enhances the reliability of the extracted kinetic parameters and is consistent with recommendations in recent literature [32–34].

The deconvolution was carried out using the open-source R package tgcd [35], applying a first-order kinetic model as recommended in recent studies [36]. The analytical expression used is based on the model 'f1' described by Bos et al. [20], which incorporates a fourth-order polynomial approximation to simulate peak asymmetry:

$$I(T) = I_m exp\left(\frac{E}{kT_m} - \frac{E}{kT}\right) exp\left[\frac{E}{kT_m}\alpha\left(\frac{E}{kT_m}\right) - \left(\frac{T}{T_m}\right)\alpha\left(\frac{E}{kT}\right)\exp\left(\frac{E}{kT_m} - \frac{E}{kT}\right)\right]$$

where I_m is the peak intensity, T_m is the peak temperature, E is the activation energy, and k is Boltzmann's constant. Here, $\alpha(x)$ is a rational function, expressed as a quotient of two fourth-order polynomials as follows:

$$\alpha(x) = \frac{a_0 + a_1 x + a_2 x^2 + a_3 x^3 + x^4}{b_0 + b_1 x + b_2 x^2 + b_3 x^3 + x^4}$$

where a_i and b_i are empirical fitting constants determined during curve deconvolution.

This model is particularly well-suited for TL glow curves exhibiting invariant peak temperatures with dose, as observed in our study. Furthermore, the adoption of first-order kinetics mitigates parameter ambiguity in overlapping regions and yields more physically meaningful kinetic parameters.

The CGCD analysis using a first-order kinetic model was applied to the TL glow curves of preheated YBB samples (preheated at 155 °C for 5 *s*), which had been irradiated with various β doses (10, 100, 200, and 500 Gy). This approach was adopted in response to the reviewer's suggestion to avoid general-order fitting for overlapping peaks. The deconvolution results for each dose are presented in Fig. 9a–d, and the corresponding kinetic parameters are summarized in Table 2.

When a preheating step (155 °C, 5 *s*) was applied prior to TL measurement, the glow curves obtained at different β doses (10, 100, 200, and 500 Gy) were deconvoluted using a first-order kinetic model, as recommended in recent studies (36). The resulting fits, shown in Fig. 9a–d, revealed between 7 and 10 distinguishable peaks depending on the dose. As expected, the shallow traps below ~130 °C were effectively eliminated by preheating, leaving well-defined deeper glow peaks in the 160–390 °C range. Activation energies (E_a) obtained from first-order fitting ranged between 1.12 and 1.95 eV, in line with values typically attributed to stable deep traps. The quality of the fits was satisfactory across all doses, with residuals indicating low deviation (FOM <1.3 %).

The frequency factor (*s*), often interpreted as the attempt-to-escape frequency, provides insight into the microscopic processes governing thermally stimulated luminescence. In both preheated and non-preheated cases analyzed here, the extracted *s* values range between

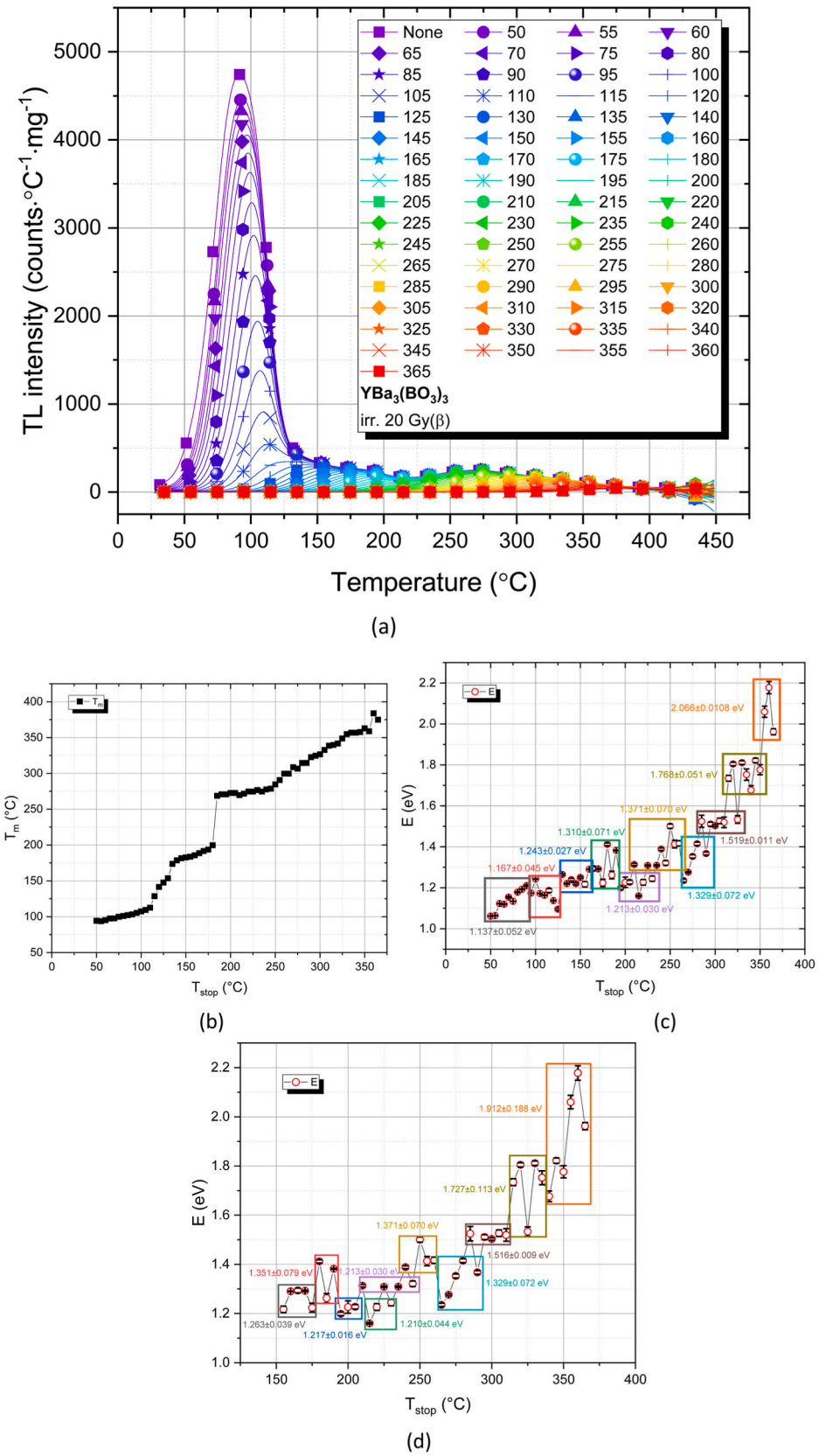

Fig. 8. (a) TL glow curves of YBB measured after successive T_{stop} steps (50–365 °C), (b) T_m vs T_{stop} plot, and (c) corresponding activation energies (E) derived from the initial rise method, revealing multiple trap levels across the studied temperature range. (d) E values obtained after preheating the sample to 100 °C prior to each T_{stop}, revealing suppression of shallow traps and enhanced resolution of deeper levels.

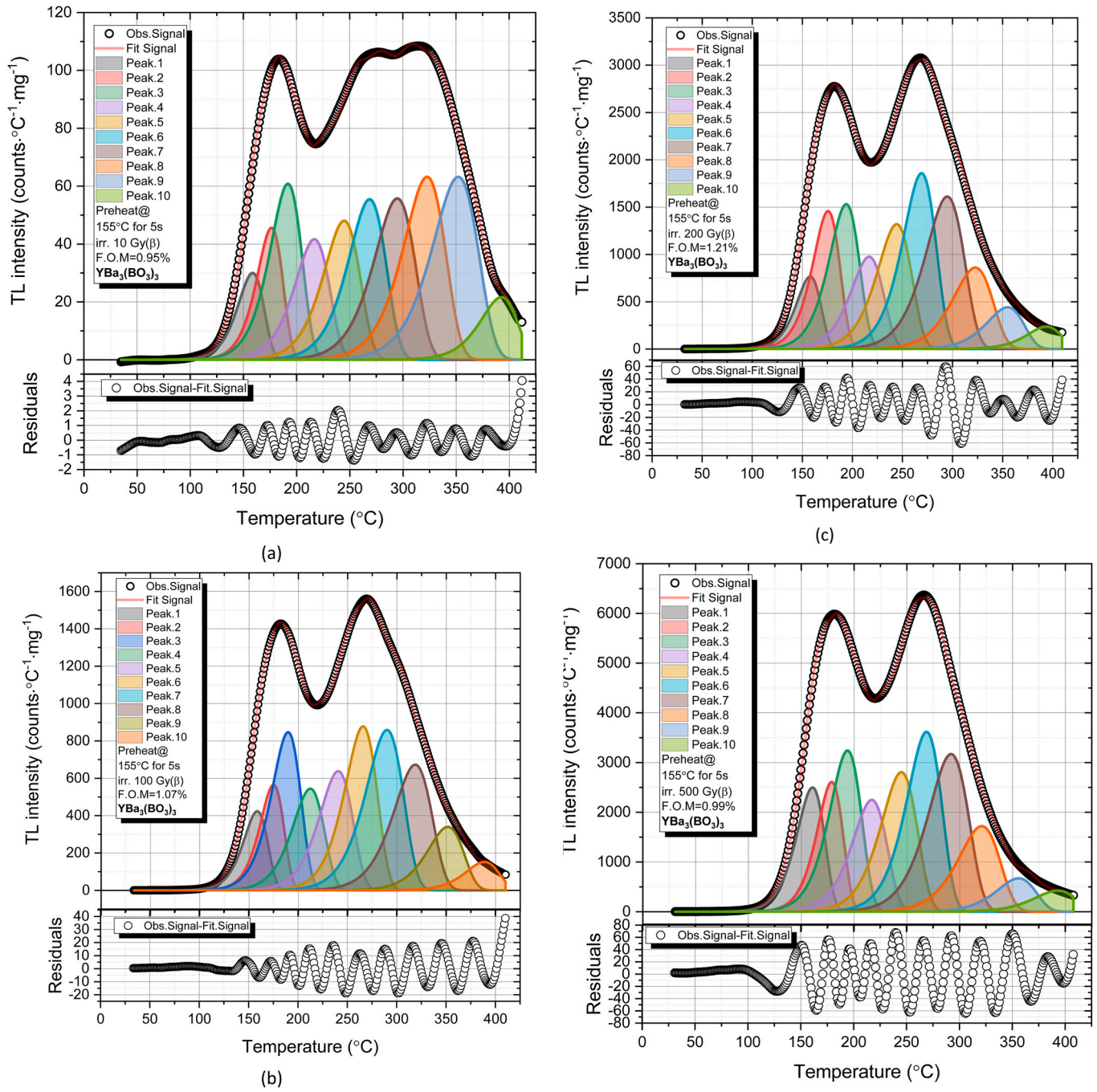

Fig. 9. CGCD deconvolution results of TL glow curves for YBB: (a–d) preheated at 155 °C for 5 *s* and irradiated with 10, 100, 200, and 500 Gy, respectively (first-order kinetics). Residuals below each curve confirm good fitting quality.

$\sim 10^{10}$ and 10^{15} s^{-1}, which are within the typical range for localized trap-release models. However, as noted by Yazan et al. [37], *s* is not solely a material constant but is also influenced by the complexity of the trapping sites, their spatial correlation with recombination centers, and the distribution of potential barriers. The broader range and higher s values observed in deeper traps (especially above 1.5 eV) suggest more complex or spatially correlated trapping environments. This supports the presence of both simple and complex trap configurations in the YBB lattice, even within the framework of first-order kinetics.

The CGCD analysis applied to preheated TL glow curves revealed well-resolved high-temperature peaks associated with thermally stable deep traps. The elimination of shallow components below ~130 °C through the preheating step enabled a clearer identification of persistent trapping centers in the 160–390 °C range. The activation energies and symmetry factors obtained from first-order kinetic modeling confirmed that these deeper traps are structurally robust and energetically isolated. This behavior supports the suitability of undoped YBB for dosimetric applications requiring long-term charge retention and thermal stability, such as high-dose or high-temperature radiation detection.

The activation energies and thermal stability trends observed from the CGCD analysis (Fig. 9; Table 2) are in good agreement with the energy levels obtained via the T_M–T_{stop} method using the initial rise approach (Fig. 8c and d). In particular, shallow traps below ~130 °C with activation energies around 1.06–1.13 eV identified in the non-

Table 2
Kinetic parameters obtained from CGCD analysis of the preheated TL glow curves of YBB (preheated at 155 °C for 5 *s*) irradiated with different β doses (a)10, (b)100, (c) 200, and (d) 500 Gy. The deconvolution was performed using a first-order kinetic model ($b = 1$ fixed). Parameters include activation energy (E_a), peak maximum temperature (T_m), symmetry factor (μ), and frequency factor (s). Residual analysis confirms satisfactory fit quality.

(a)

	E_a (eV)	T_m (°C)	T_{m1} (°C)	T_{m2} (°C)	μ	s (s^{-1})
1st Peak	1.29	158.72	141.59	170.93	0.40	1.81×10^{14}
2nd Peak	1.41	176.52	159.48	188.64	0.40	1.02×10^{15}
3rd Peak	1.22	191.92	171.10	206.89	0.40	2.17×10^{12}
4th Peak	1.24	216.85	194.16	233.19	0.41	6.79×10^{11}
5th Peak	1.32	244.85	221.02	262.00	0.41	7.94×10^{11}
6th Peak	1.39	268.86	244.19	286.60	0.41	1.08×10^{12}
7th Peak	1.42	294.85	268.07	314.15	0.41	3.28×10^{11}
8th Peak	1.52	322.85	295.45	342.57	0.41	7.08×10^{11}
9th Peak	1.53	352.19	322.31	373.75	0.42	1.94×10^{11}
10th Peak	2.17	392.85	368.52	410.12	0.41	2.99×10^{15}

(b)

	E_a (eV)	T_m (°C)	T_{m1} (°C)	T_{m2} (°C)	μ	s (s^{-1})
1st Peak	1.29	158.31	141.22	170.50	0.42	1.87×10^{14}
2nd Peak	1.41	174.82	157.91	186.85	0.40	1.18×10^{15}
3rd Peak	1.22	189.62	168.99	204.44	0.42	2.55×10^{12}
4th Peak	1.24	212.18	189.91	228.21	0.41	9.18×10^{11}
5th Peak	1.32	240.45	217.01	257.32	0.42	1.04×10^{12}
6th Peak	1.50	265.70	242.87	282.05	0.40	1.28×10^{13}
7th Peak	1.42	289.97	263.64	308.95	0.41	4.29×10^{11}
8th Peak	1.52	318.53	291.51	337.97	0.42	8.91×10^{11}
9th Peak	1.81	351.66	326.16	369.88	0.42	4.27×10^{13}
10th Peak	2.17	388.70	364.67	405.77	0.40	3.83×10^{15}

(c)

	E_a (eV)	T_m (°C)	T_{m1} (°C)	T_{m2} (°C)	μ	s (s^{-1})
1st Peak	1.29	157.91	140.84	170.08	0.42	1.94×10^{14}
2nd Peak	1.26	175.74	156.87	189.25	0.42	2.03×10^{13}
3rd Peak	1.22	193.85	172.85	208.94	0.42	1.90×10^{12}
4th Peak	1.24	216.85	194.15	233.19	0.42	6.79×10^{11}
5th Peak	1.32	244.26	220.49	261.38	0.41	8.23×10^{11}
6th Peak	1.50	269.14	246.03	285.70	0.40	1.03×10^{13}
7th Peak	1.41	294.85	268.07	314.16	0.42	3.28×10^{11}
8th Peak	1.52	322.85	295.45	342.57	0.42	7.08×10^{11}
9th Peak	1.81	355.06	329.29	373.48	0.40	3.52×10^{13}
10th Peak	2.17	393.85	369.45	NA	NA	2.81×10^{15}

(d)

	E_a (eV)	T_m (°C)	T_{m1} (°C)	T_{m2} (°C)	μ	s (s^{-1})
1st Peak	1.29	157.91	140.84	170.08	0.42	1.94×10^{14}
2nd Peak	1.26	175.74	156.87	189.25	0.42	2.03×10^{13}
3rd Peak	1.22	193.85	172.85	208.94	0.42	1.90×10^{12}
4th Peak	1.24	216.85	194.15	233.19	0.42	6.79×10^{11}
5th Peak	1.32	244.26	220.49	261.38	0.41	8.23×10^{11}
6th Peak	1.50	269.14	246.03	285.70	0.40	1.03×10^{13}
7th Peak	1.41	294.85	268.07	314.16	0.42	3.28×10^{11}
8th Peak	1.52	322.85	295.45	342.57	0.42	7.08×10^{11}
9th Peak	1.81	355.06	329.29	373.48	0.40	3.52×10^{13}
10th Peak	2.17	393.85	369.45	NA	NA	2.81×10^{15}

preheated CGCD analysis correspond to the initial low-energy region seen in the T_{stop} curve (Fig. 8c), which disappears after preheating (Fig. 8d). Likewise, the mid- and high-temperature peaks ranging from 1.3 to 1.96 eV observed in both analyses align well, confirming the presence of deeper, more thermally stable traps.

This consistency between the two independent techniques—CGCD and T_M–T_{stop}—enhances the reliability of the identified trap distributions. While CGCD provides detailed peak-by-peak resolution with kinetic parameters, the T_M–T_{stop} method offers a broader, temperature-resolved perspective on trap evolution. The combined interpretation reinforces the multilevel trap structure in YBB, confirming the robustness of the experimental methodology.

5. Conclusions

This comprehensive investigation into the thermoluminescence behavior of YBB phosphor reveals a rich and complex trap structure suitable for advanced dosimetric applications. The glow curve analysis demonstrated unusually stable TL intensities across varying heating rates, a behavior attributed to thermally robust traps and effective thermal conductivity of the host lattice. Kinetic analyses performed using the Variable Heating Rate (VHR), T_M–T_{stop}, and Computerized Glow Curve Deconvolution (CGCD) methods consistently revealed multiple trapping levels with activation energies ranging from ~1.12 eV to ~1.95 eV. Preheating treatments effectively removed unstable shallow traps while preserving deep, stable ones, improving the resolution of the kinetic components. The strong agreement between T_M–T_{stop} and CGCD results confirmed the reliability of the derived

kinetic parameters and validated the use of a first-order kinetic model for preheated samples. The frequency factor (s) values, spanning from 10^{10} to 10^{15} s^{-1}, further indicated the coexistence of both simple and complex recombination centers within the borate lattice.

Overall, the YBB phosphor demonstrates thermally stable TL performance with well-isolated deep traps, making it a promising candidate for high-temperature or high-dose radiation dosimetry. To extend its applicability toward low-dose personal dosimetry (0.01–1 Gy), further enhancements in TL sensitivity− possibly through rare-earth doping, co-doping, or sensitization strategies− merit future investigation. Additional studies will also focus on the long-term fading behaviour and precise dose-response characteristics to evaluate its practical viability.

CRediT authorship contribution statement

E. Aymila Çin: Software, Methodology, Investigation, Formal analysis. **K. Bulcar:** Software, Formal analysis. **Jabir Hakami:** Software, Data curation, Conceptualization. **U.H. Kaynar:** Methodology, Investigation, Formal analysis. **M. Sharahili:** Methodology, Data curation. **O. Madkhali:** Software, Conceptualization. **D. Somaily:** Investigation, Conceptualization. **Rachid Karmouch:** Investigation, Data curation. **D. A. Jabali:** Methodology, Investigation. **M.B. Coban:** Software, Methodology. **G.M. Güngör Price:** Methodology, Data curation. **M. Topaksu:** Methodology, Investigation. **N. Can:** Writing – review & editing, Writing – original draft, Supervision.

Declaration of competing interest

The authors declare that they have no known competing financial interests or personal relationships that could have appeared to influence the work reported in this paper.

Acknowledgements

The authors gratefully acknowledge the funding of the Deanship of Graduate Studies and Scientific Research, Jazan University, Saudi Arabia, through Project number: (JU- 20250218 -DGSSR- RP -2025).

References

[1] S. Verma, K. Verma, D. Kumar, B. Chaudhary, S. Som, V. Sharma, V. Kumar, H. C. Swart, Recent advances in rare Earth doped alkali-alkaline Earth borates for solid state lighting applications, Phys. B Condens. Matter 535 (2018) 106–113, https://doi.org/10.1016/j.physb.2017.06.073.

[2] M. Farooq, M.H. Rasool, H. Rafiq, I. Nazir, S. Rubab, Synthesis, characterization and optical tuning of $Sm^{3}+$ doped $NaZnPO_4$ phosphors for white LED technology, Ceram. Int. 50 (2024) 21118–21129, https://doi.org/10.1016/j.ceramint.2024.03.221.

[3] Y.R. Parauha, N.T. Kalyani, S.J. Dhoble, Recent trends in rare Earth doped luminescent materials: a review, J. Mol. Struct. 1347 (2025) 143190, https://doi.org/10.1016/j.molstruc.2025.143190.

[4] H.J. Alathlawi, A. Barad, O. Madkhali, G. Souadi, M. Sharahili, J. Hakami, S. Balci, U.H. Kaynar, M. Topaksu, N. Can, Intrinsic thermoluminescence and anomalous heating rate effects in undoped $K_7SrY_2(B_5O_{10})_3$ phosphors: a combined Tm–Tstop and GOK deconvolution study, Appl. Radiat. Isot. 225 (2025) 112092, https://doi.org/10.1016/j.apradiso.2025.112092.

[5] R. Kiran, N. Kamath, M.I. Sayyed, A.H. Almuqrin, S.D. Kamath, A review of recent developments in rare earth-doped nanophosphors for emerging technological applications, RSC Adv. 15 (2025) 20040–20060, https://doi.org/10.1039/D5RA03126E.

[6] O. Madkhali, Thermoluminescence characterization of europium doped gadolinium aluminum borate phosphors: impacts of europium doping under beta irradiation, Ceram. Int. 51 (2025) 11603–11617, https://doi.org/10.1016/j.ceramint.2025.01.015.

[7] M. Oglakci, Z.G. Portakal-Uçar, S. Akça-Özalp, V. Correcher, J.F. Benavente, M. Sonsuz, N. Can, Y.Z. Halefoglu, M. Topaksu, Thermoluminescence behavior of Ce^{3+} doped lanthanum tri-borate phosphor for dosimetry applications, Ceram. Int. 49 (2023) 36092–36102, https://doi.org/10.1016/j.ceramint.2023.08.288.

[8] R. Chen, S.W.S. McKeever, Theory of Thermoluminescence and Related Phenomena, World Scientific, 1997, https://doi.org/10.1142/2781.

[9] S.W.S. McKeever, Thermoluminescence of Solids, Cambridge University Press, 1985, https://doi.org/10.1017/CBO9780511564994.

[10] A.J.J. Bos, Thermoluminescence and Thermally Stimulated Processes in Soli, Delft University Pre, Delft, 2006.

[11] G. Souadi, K. Bulcar, Ü.H. Kaynar, M. Ayvacikli, M. Topaksu, S. Cam-Kaynar, N. Can, Anomalous dose behaviour of thermoluminescence glow curves and kinetic analysis of beta irradiated $YAl_3(BO_3)_4$:Tb phosphor, Appl. Radiat. Isot. 194 (2023) 110686, https://doi.org/10.1016/j.apradiso.2023.110686.

[12] Ü.H. Kaynar, M. Oglakci, K. Bulcar, S. Benourdja, M. Bakr, M. Ayvacikli, A. Canimoglu, M. Topaksu, N. Can, Comparison of thermoluminescence characteristics of undoped and europium doped $YAl_3(BO_3)_4$ phosphor synthesized by combustion method: anomalous heating rate, dose response and kinetic analyses, Radiat. Phys. Chem. 204 (2023) 110657, https://doi.org/10.1016/j.radphyschem.2022.110657.

[13] A.S. Altowyan, Ü.H. Kaynar, K. Bulcar, M. Oglakci, Z.G. Portakal-Uçar, J. Hakami, M. Topaksu, N. Can, Unusual heating rates, dose responses and kinetic parameters detected on thermoluminescence from $YAl_3(BO_3)_4:Sm^{3+}$ phosphors, Ceram. Int. 49 (2023) 33291–33304, https://doi.org/10.1016/j.ceramint.2023.08.038.

[14] L. Liu, Y. Zhang, J. Hao, C. Li, Q. Tang, C. Zhang, Q. Su, Thermoluminescence characteristics of terbium-doped $Ba_2Ca(BO_3)_2$ phosphor, Phys. Status Solidi 202 (2005) 2800–2806, https://doi.org/10.1002/pssa.200521199.

[15] Y. Alajlani, M. Oglakci, U.H. Kaynar, M. Ayvacikli, Z.G. Portakal-Uçar, M. Topaksu, N. Can, Thermoluminescence study and evaluation of trapping parameters of samarium doped barium silicate phosphor, J. Asian Ceram. Soc. 9 (2021) 291–303, https://doi.org/10.1080/21870764.2020.1864898.

[16] A.S. Altowyan, U.H. Kaynar, C. Gök, H. Aydin, J. Hakami, M.B. Coban, A. Canimoglu, N. Can, Photoluminescence characteristics and Judd–Ofelt analysis of $YBa_3(BO_3)_3:Tb^{3+}$ phosphors co-doped with Li^{+}, Na^{+}, and K^{+}, J. Lumin. 286 (2025) 121380 https://doi.org/10.1016/j.jlumin.2025.121380.

[17] M. Bakr, Z.G. Portakal-Uçar, M. Yüksel, Ü.H. Kaynar, M. Ayvacikli, S. Benourdja, A. Canimoglu, M. Topaksu, A. Hammoudeh, N. Can, Thermoluminescence properties of beta particle irradiated $Ca_3Al_2O_6$ phosphor relative to environmental dosimetry, J. Lumin. 227 (2020) 117565, https://doi.org/10.1016/j.jlumin.2020.117565.

[18] N. Can, P.D. Townsend, Y. Wang, Analytical benefits from logarithmic displays of luminescence sensitivity, Vacuum 238 (2025) 114273, https://doi.org/10.1016/j.vacuum.2025.114273.

[19] O. Madkhali, K. Bulcar, A. Barad, T. Zelai, G. Souadi, H.J. Alathlawi, U.H. Kaynar, M. Topaksu, N. Can, Thermoluminescence behaviour and kinetic analysis of a novel Tb^{3+}-Doped $LaCa_4O(BO_3)_3$ phosphor: impacts of heating rates and dose, Mater. Sci. Semicond. Process. 187 (2025) 109132, https://doi.org/10.1016/j.mssp.2024.109132.

[20] A. Bos, Thermoluminescence as a research tool to investigate luminescence mechanisms, Materials 10 (2017) 1357, https://doi.org/10.3390/ma10121357.

[21] A.S. Altowyan, M. Sonsuz, U.H. Kaynar, J. Hakami, Z.G. Portakal-Uçar, M. Ayvacikli, M. Topaksu, N. Can, Synthesis and thermoluminescence behavior of novel Sm^{3+} doped $YCa_4O(BO_3)_3$ under beta irradiation, Ceram. Int. 50 (2024) 19681–19691, https://doi.org/10.1016/j.ceramint.2024.03.089.

[22] G. Souadi, Ü.H. Kaynar, M. Sonsuz, S. Akça-Özalp, M. Ayvacikli, M. Topaksu, O. T. Ozmen, N. Can, Unravelling the impact of unusual heating rate, dose-response and trap parameters on the thermoluminescence of Sm^{3+} activated $GdAl_3(BO_3)_4$ phosphors exposed to beta particle irradiation, Radiat. Phys. Chem. 213 (2023) 111211, https://doi.org/10.1016/j.radphyschem.2023.111211.

[23] G. Kitis, J.W.N. Tuyn, A simple method to correct for the temperature lag in TL glow-curve measurements, J. Phys. D Appl. Phys. 31 (1998) 2065–2073, https://doi.org/10.1088/0022-3727/31/16/017.

[24] W. Hoogenstraaten, Electron traps in zinc-sulphide phosph, Philips Res. Rep. 13 (1958) 515–693.

[25] G. Souadi, K. Bulcar, S. Akça-Özalp, U.H. Kaynar, H.J. Alathlawi, O. Madkhali, M. Sharahili, D.A.E. Somaily, M. Topaksu, N. Can, Anomalous heating rate dependence and kinetic analysis of Eu^{3+}-activated $K_7SrY_2(B_5O_{10})_3$ borate phosphors, Ceram. Int. (2025), https://doi.org/10.1016/j.ceramint.2025.09.091.

[26] Y. Alajlani, M. Oglakci, A. Barad, U.H. Kaynar, M. Topaksu, A. Canimoglu, N. Can, Anomalous heating rate and kinetic analysis in the thermoluminescence of $GdCa_4O(BO_3)_3$, Radiat. Phys. Chem. 232 (2025) 112614, https://doi.org/10.1016/j.radphyschem.2025.112614.

[27] A. Bohun, Thermoemission und Photoemission von Natriumchlorid, Czechoslov, J. Phys. 4 (1954) 91–93, https://doi.org/10.1007/BF01688114.

[28] A.H. Booth, Calculation of electron trap depths from Thermoluminescence Maxima, Can. J. Chem. 32 (1954) 214–215, https://doi.org/10.1139/v54-027.

[29] J.F. Benavente, J.M. Gómez-Ros, V. Correcher, Characterization of the thermoluminescence glow curve of $Li_2B_4O_7$:Cu,Ag, Radiat. Meas. 137 (2020) 106427, https://doi.org/10.1016/j.radmeas.2020.106427.

[30] Z.G. Portakal-Uçar, M. Oglakci, V. Correcher, M. Sonsuz, N. Can, Y.Z. Halefoglu, M. Topaksu, A thermoluminescence study of Tb^{3+} doped LaB_3O_6: dosimetric characteristics and kinetic parameters, J. Lumin. 253 (2023) 119493, https://doi.org/10.1016/j.jlumin.2022.119493.

[31] G.F.J. Garlick, A.F. Gibson, The electron trap mechanism of luminescence in sulphide and silicate phosphors, Proc. Phys. Soc. 60 (1948) 574–590, https://doi.org/10.1088/0959-5309/60/6/308.
[32] G.S. Polymeris, G. Kitis, N.C. Tsirliganis, Correlation between TL and OSL properties of CaF_2:N, Nucl. Instruments Methods Phys. Res. Sect. B Beam Interact. with Mater. Atoms 251 (2006) 133–142, https://doi.org/10.1016/j.nimb.2006.05.023.
[33] G.I. Dallas, G.S. Polymeris, D. Afouxenidis, N.C. Tsirliganis, N.F. Tsagas, G. Kitis, Correlation between TL and OSL signals in $KMgF_3$:Ce^{3+}: bleaching study of individual glow-peaks, Radiat. Meas. 45 (2010) 537–539, https://doi.org/10.1016/j.radmeas.2009.11.008.
[34] R.K. Gartia, T.T. Singh, T.B. Singh, Optically stimulated luminescence (OSL) of Lu2SiO5:Ce powder: a preliminary study, Nucl. Instruments Methods Phys. Res. Sect. B Beam Interact. with Mater. Atoms 269 (2011) 30–33, https://doi.org/10.1016/j.nimb.2010.10.008.
[35] J. Peng, Z. Dong, F. Han, Tgcd: an R package for analyzing thermoluminescence glow curves, SoftwareX 5 (2016) 112–120, https://doi.org/10.1016/j.softx.2016.06.001.
[36] Edwin J. Pilco, Nilo F. Cano, Jorge S. Ayala-Arenas, J.A. Suárez-Navarro, J. F. Benavente, Numerical studies to validate mathematical models based on first-order and general-order kinetic approaches for fitting TL glow curves, Phys. Lett. 553 (2025) 130674, https://doi.org/10.1016/j.physleta.2025.130674.
[37] H. Yazan, Z.G. Portakal-Uçar, S. Akça, M. Topaksu, P.D. Townsend, N. Can, Thermoluminescence of Ce and Nd co-doped CaF_2 phosphors after beta irradiation, J. Lumin. 234 (2021) 117949, https://doi.org/10.1016/j.jlumin.2021.117949.